# A Stationary Core with a One-sided Jet in the Center of M81

M. F. Bietenholz and N. Bartel
Department of Physics and Astronomy, York University, Toronto, M3J 1P3, Ontario, Canada

and M. P. Rupen
National Radio Astronomy Observatory, Socorro, New Mexico 87801, USA

(accepted for publication in the *Astrophysical Journal*)

## ABSTRACT

The nucleus of the nearby spiral galaxy M81 was observed at 8.3 GHz with a global VLBI array at 20 epochs over four and a half years, with a linear resolution at the source of about 2000 AU or 0.01 pc. Phase-referenced mapping with respect to the geometric center of supernova 1993J in the same galaxy enabled us to find, with a standard error of about 600 AU, a stationary point in the source south-east of the brightness peak. We identify this point as the location of the core and the putative black hole at the gravitational center of the galaxy. The $2\sigma$ upper bound on the core's average velocity on the sky is $\leq 40$ $\mu$as yr$^{-1}$ or $\leq 730$ km s$^{-1}$ (relative to the center of SN1993J, in excess of galactic rotation). A short, one-sided jet extends towards the north-east from the core, in projection approximately in line with the rotation axis of the galaxy, and towards the well-known extended emission 1 kpc further out. The orientation of the jet varies smoothly, with timescales of about one year, and an rms of 6°, around its mean position angle of 50°. Occasionally the jet appears to bend to the east. The length of the jet is only about 1 mas (3,600 AU), and varies with an rms of about 20% from epoch to epoch. The inferred speeds are below $0.08c$. The total flux density of the core-jet varies erratically, changing on occasion by a factor of two over a few weeks, without any significant changes in the source size and orientation. The inferred velocity of the plasma flow is $> 0.25c$. The results are consistent with a model in which plasma condensations with short lifetimes are ejected relativistically from the core on a timescale of less than a few weeks. The condensations travel along a tube whose pattern and geometry are also variable but only on a timescale of about one year. The central engine of M81 has qualitative similarities to those of powerful active galactic nuclei of radio galaxies and quasars, and may also represent in power and size a scaled-up version of the largely hidden nucleus in our own Galaxy.

*Subject headings:* galaxies: individual (M81) — galaxies: nuclei — radio continuum: galaxies

## 1. Introduction

The nearby galaxy M81 (NGC 3031, 0951+693) is a grand-design spiral that resembles our own Galaxy in type, size, and mass. Like our Galaxy, it contains a nuclear radio source that is most likely associated with a supermassive black hole in the gravitational center of the galaxy. M81 also shares some characteristics with radio galaxies and quasars. Its nucleus has a high X-ray luminosity ($\sim 1.7 \times 10^{40}$ erg s$^{-1}$, Elvis & Van Speybroeck 1982) and a non-stellar UV continuum (Ho, Fillipenko & Sargent 1996). Optical spectroscopy shows broad H$\alpha$ lines (Peimbert & Torres-Peimbert 1981) and double peaked broad other emission lines, which in galaxies with an active galactic nucleus (AGN) are almost always associated with jets (Bower et al. 1996). The central radio source in our Galaxy, Sgr A$^*$, is largely hidden behind scattering clouds of gas that have so far allowed only the crudest determinations of its intrinsic size and orientation (Lo et al. 1998; Krichbaum et al. 1998). M81's central radio source, on the other hand, is virtually unaffected by scatter broadening at most radio frequencies. M81 is also, at a distance of 3.63 Mpc (Freedman et al. 1994), the nearest spiral galaxy with a central compact radio source, and, with the radio galaxy Cen A (Tingay et al. 1998), the nearest galaxy with an AGN altogether. With a radio luminosity of $10^{37.5}$ ergs s$^{-1}$, the nucleus of M81 could therefore be both a more readily observable analog to Sgr A$^*$, and a useful link between our galactic center and the more powerful nuclei of radio galaxies and quasars.

Previous observations have confirmed that M81*[1] is similar to typical AGN in terms of its very-long-baseline interferometry (VLBI) brightness temperature of $\sim 10^{10}$ K at 8 GHz and its radio spectrum, which is slightly inverted. Its spectral index, $\alpha$ ($S \propto \nu^{\alpha}$), is about +0.2 from a frequency of $\sim$ 1 GHz to its turnover frequency of $\sim$ 100 GHz (Reuter & Lesch 1996; Bartel et al. 1982, B82 hereafter). The high turnover frequency suggests an unusually small source; this is consistent with VLBI observations which gave a size of 700 AU $\times$ 300 AU at 22 GHz (Bietenholz et al. 1996, hereafter Paper I; see also Bartel, Bietenholz & Rupen 1995, Bietenholz et al. 1994, B82, and Kellermann et al. 1976). It is larger at lower frequencies, with the length of the major axis being proportional to $\nu^{-0.8}$ between 2.3 GHz and 22 GHz. The orientation of M81* is also frequency dependent, bending from $\sim$40° at 22 GHz to $\sim$75° at 2.3 GHz. This result, combined with a slight asymmetry in the brightness within the source with the source being fainter towards the north-east (NE), suggests a typical, albeit tiny, core-jet source with a bent jet. One surprise is that no significant changes in the size and orientation of M81* were seen between the epochs of the observations in 1981 and 1993 (Paper I, B82), giving an extremely low nominal expansion velocity of $-60 \pm 60$ km s$^{-1}$. Such low velocities are unusual for core-jet sources where plasma condensations are ejected relativistically. They can perhaps be understood if the plasma condensations are ejected relativistically from the core, but then follow nearly identical trajectories, and are ejected frequently enough to keep the integrated flux distribution fairly constant. Here we report on observations from

[1]Following Melia (1992) and others we adopt the convention of adding an asterisk to the name of the galaxy when referring to the VLBI source in the galaxy's center.

20 epochs of VLBI observations of M81*, taken between 1993 and 1997. Using phase referencing, these observations have allowed us to identify astrometrically a small stationary region in the south-west (SW) of the source as the probable core, and to detect and characterize clear structural variability in the jet.

We describe the observations and data reduction in sections §2 and 3. In §4 we give the radio lightcurve determined with the NRAO[2] Very Large Array (VLA). In §5 we present six representative images illustrating the structural variability. In §6 we examine this variability in more detail by fitting one- and two-component models in the $u$-$v$ plane. In §7 we give our astrometric results from phase-referencing to supernova 1993J, and identify the stationary core in the SW and the variable jet. In §8 we discuss the properties of the jet. In §9 we discuss our results in terms of a core-jet model for M81*, and finally, in §10 we summarize our conclusions. (For a preliminary presentation of some of these results, see Bietenholz, Bartel & Rupen 1997).

## 2. Observations

The observations were made with a global array of between 11 and 18 telescopes (see Table 1) with a total time of 12 to 18 hours for each run, giving us exceptionally good $u$-$v$ coverage. Each telescope was equipped with a hydrogen maser as a time and frequency standard. The data were recorded with the VLBA (Very Long Baseline Array) and either the MKIII or the MKIV VLBI systems with sampling rates of 128 or 256 Mbits per second. M81* was observed as a phase reference source for the continuing multi-frequency program of VLBI observations of SN1993J, located $\sim 170''$ away towards the south south-west in a spiral arm of the galaxy (Bartel et al. 1999, 1994). In general, a cycle time of $\sim$ 3 min was used, in which M81* was observed for 70s and SN1993J for 120 s (a longer cycle time was used only during the first three epochs). In addition the sources OQ208 and 0954+658 were observed occasionally during each session as fringe finders and calibrator sources. In each session data at two to four frequencies out of a total of six (1.7, 2.3, 5.0, 8.3, 15, and 22 GHz) were recorded, with 5.0 and 8.3 GHz being the standard frequencies used in (almost) every session. Here we report on the VLBI observations at 8.3 GHz only, where we always recorded right (IEEE convention), and for later runs also left circular polarization.

The phased VLA was used in all of these VLBI observations, and the (simultaneous) interferometric data from it provided accurate flux measurements at 8.3 GHz of M81 and SN1993J. Both senses of circular polarization were recorded with a bandwidth of 50 MHz per polarization. During the four and a half years of observations data were taken in all four standard, as well as in various hybrid VLA configurations. The dates of observations and the array configurations are given in Table 2.

[2]The National Radio Astronomy Observatory is a facility of the National Science Foundation operated under cooperative agreement by Associated Universities, Inc.

## 3. Data Reduction

The VLBI data were correlated using the VLBA processor in Socorro, NM. Further data reduction, i.e. fringe-fitting, editing, and initial calibration, was done with NRAO's software package, AIPS, in the usual way. The final calibration was done by starting with a single Gaussian model and then iteratively self-calibrating the complex antenna gains. Phases were derived first, with a solution interval of $\sim 1$ min, and then amplitudes, with final solution intervals of 1 to 2 h.

In order to more precisely describe the structural properties of the nucleus, we turned to model-fitting. We first averaged the data for each epoch into scans of $\sim 1$ min duration. We then used the AIPS least-squares fitting program OMFIT which simultaneously fits the time-varying antenna gains (self-calibrates) and solves for the model parameters. Solving again for the antenna gains at the same time as solving for the source parameters is essential because the two will generally be correlated. The resulting model parameters were derived in conjunction with antenna gains which had solution intervals of 1 min in phase and 1 h in amplitude.

Total flux densities were obtained from the interferometric VLA data from the M81* pointings of our observing runs. In particular, we derived the flux densities from CLEAN images made from the fully phase-selfcalibrated and naturally weighted data. The flux densities are on the scale of Baars et al. (1991). In all cases the internal uncertainties in the VLA flux densities, including the possible effect of extended structure[3], were dominated by the standard error in the VLA calibration, which we conservatively assume to be 5%.

## 4. VLA total flux densities

We list the total flux densities of M81* at 8.3 GHz and their mean and rms (root-mean-square) scatter about the mean for 20 epochs in Table 2. These same flux densities are graphed in Figure 1*a*. For comparison, we show in Figure 1*b* the flux densities of SN1993J, which were derived from SN1993J pointings which alternated with M81* pointings in the same observing runs, and were calibrated using the same gain amplitudes, and so any calibration problems in the M81* data would almost certainly be apparent in the flux densities measured for SN1993J. Since, however, the latter show only the expected smooth decline to well within the errors, we are confident that our measurements of the variable flux densities of M81* are reliable and correct within the quoted errors. All our uncertainties are one standard error unless otherwise noted.

The flux densities of M81* fluctuate strongly. They vary by over a factor of 2 from 81 mJy to 189 mJy, with the rms deviation being 23% of the mean of 127 mJy. The variation appears random

[3]There is a small amount of extended emission near M81* on arcsecond scales which in principle could contaminate our results from compact array configurations. However, the total flux density of any such emission is less than a few percent of that of M81* (Bartel et al. 1995; Kaufman et al. 1996), excluding it as a source of significant error.

from epoch to epoch. The degree of variability and the mean flux density are consistent with those reported by others (Ho et al. 1999; Crane, Guiffrida & Carlson 1976).

We examined our data for possible flux density variations during the course of an observing run. No significant variations were found — For the 12 epochs we inspected, we found no changes in flux density larger than our standard errors of about 5% over the course of an observing run, or, extrapolated, 10% per day. We therefore do not confirm the occasional changes of up to 60% (with inferred standard errors of up to ±30%) reported for similar short periods by Ho et al. (1999).

## 5. VLBI images

Figure 2 $a$ – $f$ show six representative images of M81*, from May 1993, June 1994, Feb. 1995, May 1995, Dec. 1996, and Nov. 1997 respectively. All the images are made with CLEAN, using uniform weighting. They are shown convolved with a common restoring beam of 0.5 mas FWHM (full width at half maximum). Even with the resolution attained with a global array, the structure is only marginally resolved. Nevertheless, it is clear that the source is extended at each of the six epochs approximately along the NE-SW axis, with its length being of order 1 mas.

We searched for signs of extended emission on spatial scales of $\sim$ 10 to 100 mas, which are resolved out with VLBI but unresolved with the VLA. For all of our observing sessions, we formed the ratio of the total flux density measured with the VLA to that measured by VLBI. This ratio for M81* shows no systematic difference to that observed for SN1993J, which physically is not expected to have any extended emission on these scales. We conclude that the flux density of any emission on scales of $\sim$ 10 to 100 mas associated with M81* is $< 8$ mJy, or $< 6\%$ of the total flux density.

In addition to the extension of $\sim 1$ mas, slight changes in the structure are visible: the images shown in Fig. 2 show that the size of the source along the NE-SW axis as well as the orientation of its major axis are changing. For example, both changes in extension and orientation are evident between Figs. 2$a$ and $b$.

Are the variations significant given that the source size is generally smaller than the minimum fringe spacing of the array? Could they for instance be artifacts of the self-calibration process? To investigate these questions, we searched for a signature of the different sizes and orientations in the "raw" data, namely the $u$-$v$ data which have only been self-calibrated with a preliminary model common to both epochs, and were therefore still unaffected by the individual iterative self-calibration processes for each epoch. As an example of the size change we show in Figure 3$a$ the visibility amplitudes as a function of the $u$-$v$ distance for our observing runs of May 1993 and June 1994 (see Fig. 2$a, b$ for the images). Clearly the visibility curve for the data of the latter epoch is narrower, showing that the source is indeed more extended at that epoch.

Similarly, for the change in orientation, we show in Fig. 3$b$ the average visibility amplitude in an

annulus of $u$-$v$ distances between 200 M$\lambda$ and 260 M$\lambda$ as a function of $u$-$v$ position angle (p.a.) for the same two epochs. The limits of the annulus were chosen to display the most significant variation of amplitude with $u$-$v$ p.a. while excluding the noisier and less frequently sampled outermost regions of the $u$-$v$ plane. These curves show a minimum and a pronounced maximum which indicate that the source is not circular. There is a clear displacement of one curve with respect to the other of about 10 to 20° of $u$-$v$ p.a. Since the minimum occurs at the p.a. of the major axis, the displacement indicates different orientations of the source at these two epochs. Furthermore, the minimum in the June 1994 data is deeper than in the May 1993 data by about 30% while the maxima have about the same relative correlated flux densities. This is a signature of differing degrees of source ellipticity.

Since, again, these data have not been self-calibrated to convergence for each individual epoch, the difference between the two curves in each of the parts of Figure 3 cannot be ascribed to any divergence in the self-calibration process, and therefore are highly significant. In fact, the self-calibration process generally caused only small changes in our derived values, in particular, the plots shown in Fig. 3 are virtually identical after self-calibration. We conclude that the size and orientation of the source can vary significantly. For the first time, structural changes from one epoch to another have been shown in the ultracompact nucleus of M81.

## 6. VLBI model fitting

### 6.1. One-component model and structural variability

To investigate the structural variability more quantitatively we employ modelfitting in the $u$-$v$ plane, which gives results which are not dependent on convolution with a restoring beam. First, we fit only a single elliptical Gaussian to the data. The results for 20 epochs are shown in Table 3. Both the size and the p.a. of the Gaussian vary, by up to 0.46 mas (i.e. 100%) and 15° respectively.

We determined the standard errors in the fit parameters as follows. We divided an individual data set into three roughly equal parts in time. We repeated the model fit for each of these time periods, and thus obtained three largely independent estimates of the model parameters. The standard error of each parameter is taken as the rms of these three estimates scaled by $1/\sqrt{3}$. Because of the small number (ie. $n=3$) statistics for each individual epoch, we quote only an average standard error estimate derived from six representative epochs. In fact, we expect that this standard error estimate represents, if anything, an over-estimate of the true uncertainty because a disproportionately better fit, and thus smaller errors, are possible when using all the data simultaneously. We consider this procedure slightly superior to that used in Paper I[4], and it yields consistent or slightly

[4]In Paper I, we based our computation of the standard error on the increase in $\chi^2$, which requires an estimate of the number of degrees of freedom which is only approximately known.

larger standard errors.

For each epoch the fit model parameter estimates and their standard errors are listed in Table 3. In addition the means of the parameter estimates, their standard errors, and their rms values are given at the bottom of the respective columns in the same table.

### 6.2. Two-component model and structural variability

Figure 2 shows that the source is slightly asymmetrical. A single elliptical Gaussian therefore provides only an approximate fit to the data. We can quantify the asymmetry of the source by fitting a point source in addition to the elliptical Gaussian; we use a point source because it is the simplest enhancement to the Gaussian model. In all cases we find that this addition causes a significant decrease in $\chi^2_\nu$ (reduced $\chi^2$), typically by $\gtrsim 10\%$ (where the number of degrees of freedom in the fit ranges from $\sim 500$ to $10,000$). Still more complex models did not improve the fit sufficiently to warrant their consideration, given the limited resolution of our observations. The standard errors of the fit parameters were determined as described for the one-component model. The results of these new fits are also listed in Table 3 and are plotted in Figure 4.

At all epochs the elliptical Gaussian is the dominant component while the point source has only 2 to 13% of the total flux density. The point source is always located NE of the elliptical Gaussian. Tests in which we inverted the flux density ratio of the two components and attempted to fit a faint elliptical Gaussian and a dominant point source to the SW instead gave poorer fits, confirming our finding in Paper I that the source becomes fainter towards the NE.

Apart from the minor axis of the elliptical Gaussian, which remains largely unresolved, all parameters vary by more than three times their standard errors. The largest relative variations are found for the parameters of the additional point source. The variations of the flux density, separation from the elliptical Gaussian, and position angle are all larger than the variations of the equivalent parameters of the elliptical Gaussian. Each of the three pairs is plotted for better comparison in a panel of Figure 4.

Of the six curves, those of the p.a. of the orientation of the elliptical Gaussian and the p.a. of the position of the point source with respect to the Gaussian (Fig. 4*b*) appear to be the smoothest. The former p.a. varies smoothly between about 40° and 60° and the latter between about 45° and 80°, both with a timescale of order one year.

The Gaussian and the point source are largely oriented along the NE-SW axis, with the point source closely tracking the p.a. of the Gaussian except during the period 1993-1994. This suggests that the underlying structure is mostly linear, as would be expected of a jet, but that it is significantly bent during 1993. Occasionally, apparently at times when M81* is compact, the p.a. can increase at least to 60° for the Gaussian and 80° for the point source. The emission away from the center therefore seems to be contained in a rather wide cone between about 40° and 80° on the

sky.

The variations for the separation of the point source from the Gaussian (Fig. 4*a*) and for the flux density of the point source (Fig. 4*c*) are somewhat less smooth. Finally, quite erratic fluctuations appear for the remaining two parameters, the length of the major axis and the flux density of the Gaussian (Fig. 4*a*, *c*), with timescales less than several weeks.

In order to investigate quantitatively how much the model parameters evolve in a smooth rather than a random way we performed a non-parametric test. For each of the six model parameters plotted against time in Figure 4, we computed $\mathrm{rms}_f$, which is the rms of the *changes* of the model parameter values from each epoch to the following one. If the model parameter values were randomly distributed over time, these changes would show no correlation with their respectively succeeding values. Changing the time sequence of the values would therefore make no difference to the $\mathrm{rms}_f$ value. By contrast, if the model parameter values displayed a smooth evolution, then the $\mathrm{rms}_f$ value for the observed sequence would be smaller than that for a random reordering of the values.

Based on 5,000 random reorderings of the values of each of the six parameters we found that the probability $p$ of obtaining $\mathrm{rms}_f$ values as low as those observed for the p.a.s of the Gaussian and of the position of the point source is $< 0.1\%$, confirming that these two parameters are indeed varying smoothly and not randomly from epoch to epoch. For the separation of the point source from the Gaussian and for the flux density of the point source the same statistic, $p$, is $\sim 3\%$, confirming that these parameters vary less smoothly. For the remaining parameters, the length of the major axis and the flux density of the Gaussian, $p \sim 50\%$ and 10%, respectively, confirming the more erratic nature of their variations.

The smooth evolution of some of the model parameters strongly suggests a smooth evolution of the source structure on similar timescales. While our *u*-*v* coverage varied from run to run, it varied in a non-systematic way (see Table 1) which would be very unlikely to cause the smooth variation seen in some of the model parameters. Further, though the true source structure is undoubtedly more complex than our simple model, the smooth changes in the model on a timescale of $\sim 1$ year would be very unlikely unless the true source geometry were also changing smoothly on the same timescale. In other words, not only have we detected significant temporal changes in the source structure, but, more specifically, temporal changes that are characterized by a smooth evolution in case of the orientation of the Gaussian and the point source, a somewhat less smooth evolution in case of the distance of the point source from the Gaussian, and in contrast, completely erratic fluctuations in case of the total flux density of the source. These characteristics are consistent with the behavior expected from a core-jet source, which we have already suggested in Paper I as the underlying structure in M81*

## 7. The core

### 7.1. Where is the core?

If the nucleus of M81 does have a core-jet structure, then where is the core located? Is the core to be identified with the point source, or does the core lie at the center, or perhaps near one end of the Gaussian? The most direct and reliable method of identifying the core is to determine astrometrically the motion of components in a core-jet source with respect to a "reputable" reference source. The core, being associated with a supermassive black hole, must remain (largely) stationary, while the jet may move (see Bartel et al. 1986 for such an identification of a core). For the possible core-jet source in M81 we used the geometric center of SN1993J as a reference point. Any motion between the core, taken to be the gravitational center of the galaxy, and the geometric center of SN1993J would be constrained to (1) the orbital motion of the progenitor around the gravitational center of the galaxy, (2) any peculiar motion the progenitor might have had, and (3) any motion of the center of SN1993J resulting from an asymmetry in the explosion. The velocity of (1) can be estimated independently from the HI rotation (Rots & Shane 1975) to be $250 \pm 80$ km s$^{-1}$ at p.a. $-40°$. The velocity of (2) can be expected to be $\lesssim 100$ km s$^{-1}$. And, the velocity of (3), judging from the high degree of circular symmetry of the supernova images (to within 3%, Bartel et al. 1999), can be expected to be $\lesssim 500$ km s$^{-1}$. In all, after subtracting the orbital motion (1), we would not expect the velocity difference between the core and the center of SN1993J to be larger than about 500 km s$^{-1}$.

The technique of phase-referenced mapping allowed us to determine the position of M81* with respect to the geometric center of SN1993J with high accuracy. SN1993J is located in the galaxy M81 but is physically unrelated to M81*, and therefore it can, for our purposes, define a galactic reference frame. Since the two sources are separated on the sky by only $\sim 0.3°$, the dominant sources of error in VLBI measurements of relative positions are much reduced. In particular, we estimate that the combined effects of statistical uncertainty and errors in the *a priori* coordinates of M81*, antenna coordinates, tropospheric and ionospheric delays at each station, UT1, pole position, and those caused by the variable structure of SN1993J and M81* give a standard error of $\sim 50$ $\mu$as for each coordinate and for each of the epochs (see, e.g. Marcaide and Shapiro 1984, Bartel et al. 1986, Rioja et al. 1997 for astrometric observations with similarly small standard errors).

In Figure 5 we plot the positions relative to the geometric center of SN1993J of three particular points in the two-component model for each of the 20 epochs. These three points are, from the NE to the SW, the point source, the center of the dominant Gaussian[5] and the SW half-width at half-maximum (HWHM) point of the Gaussian. It is apparent that the scatter of the positions for these three points decreases towards the SW. The rms of the positions for the point source is 600$\mu$as, that for the center of the Gaussian is 80$\mu$as, and that for the SW HWHM point is 60$\mu$as.

[5]We actually plot the position of the phase center, as determined by a single Gaussian fit. The position of the dominant Gaussian in the two component fit is shifted by a small amount from this phase center. Tests show that this shift is $20 \pm 20$ $\mu$as in each RA and Dec., and our positional standard errors include this contribution.

The gradient of the rms values along the major axis of the source indicates that the astrometrically most stable point is located close to the SW end of the Gaussian. In fact, we can locate the stable point more precisely: in Figure 6 we plot the positional rms as a function of location along the major axis of the Gaussian. The minimum in the curve indicates the most stable point in the model geometry. That point is located at $0.6 \pm 0.3$ FWHM from the center of the Gaussian towards the SW, i.e. close to the 35% contour of the Gaussian. The rms of the positions of this point on the sky is only 58 $\mu$as, approximately equal to the observational standard error of our astrometric position determinations of 50 $\mu$as mentioned above.

We have thus determined the most stationary point in our geometrical model of the brightness distribution. Is there any meaning to be associated with this point or could it be that the more complex true source geometry happens by chance to be least variable at this particular location? We think the latter to be unlikely, since the variability in position not only reaches a minimum at that point, but is consistent with being zero, which would be unlikely to occur by chance. Thus, we can conclude that we have identified a real, stationary part of the brightness distribution.

Can this stationary point be identified with the core? Since the core is expected to be a compact component, it might be asked why we do not parameterize the source with a compact component representing the core. However, no particular core component is apparent in the brightness distribution at any of the 20 epochs, and, as mentioned in §6.2, when we attempted to fit a model consisting of a point source and an elliptical Gaussian to the NW of it, we obtained poorer fits.

Therefore, any core component that may be hidden in the brightness distribution has to be rather weak. It follows that the brightness distribution we see is dominated by emission from the jet. It then also follows that it is emission from the jet, which mostly determines the size and location of the model components which we use to parameterize the brightness distribution, and thus which mostly determines the location of our stationary point. This point is either the core itself, or the turn-on point of the jet. Even in the latter case, we consider it physically unlikely that the turn-on point is at any significant distance from the core. We therefore identify the stationary point with the *location* of the core with considerable confidence.

We plot the location of the core in Figure 5. Note that the uncertainty in the core position is dominated by the uncertainty of locating the stationary point within our model, rather than by measurement uncertainties of our positions. It is remarkable that, despite the simple structure of our geometric model, we can identify a point in it which is stationary — this result suggests that our model describes the source geometry reasonably well even for a resolution significantly smaller than that obtained for the images. The location of the core within the brightness distribution allows us to determine that $\lesssim 25\%$ of the emission comes from the core, and $\gtrsim 75\%$ from the jet, whose properties we will discuss further in §8 below.

To summarize, we have found a point in the brightness distribution, which, to approximately within the observational standard errors, is at rest in the galactic reference frame. We therefore identified this point, with an uncertainty of 600 AU, with the location of the core.

### 7.2. Upper bound on the proper motion of the core

Having argued in §7.1 above that the relative velocity between the stationary core and the center of SN1993J is expected to be $\lesssim 500$ km s$^{-1}$, what in fact do we measure? For the four and a half year period the angular velocity is $9 \pm 7$ $\mu$as yr$^{-1}$ in R.A. and $10 \pm 7$ $\mu$as yr$^{-1}$ in Dec. At the distance of M81, this corresponds to $160 \pm 110$ and $170 \pm 120$ km s$^{-1}$ respectively. Subtracting the expected galactic motion of SN1993J of 250 km s$^{-1}$ at p.a. $-40°$ (§ 7.1; calculated from the HI rotation curve) and the inclination angle of the galaxy (59°), leaves a peculiar velocity of the core of M81* relative to SN1993J of $360 \pm 180$ km s$^{-1}$. This value is indeed comparable to the peculiar velocity expected for SN1993J, which we discussed earlier (§7.1). We do not, however, consider this value to be significant.

## 8. The jet

We have shown that the bulk of the emission originates in the jet, and we now proceed to discuss its characteristics. It is predominately oriented at a p.a. of 50°, and occasionally bends towards the east. The point source represents the distant end of it. How does the jet move with respect to the core? In Figure 7 we plot the positions with respect to the core of two points in the jet for each epoch: the NE HWHM point of the dominant Gaussian, which represents the inner jet, and the point source, which represents the end of the jet. This figure is similar to Figure 5, but the reference point is now taken to be the core position, rather than the geometric center of SN1993J. Again, it can clearly be seen that the inner jet as well as the end of the jet move, over a range of 0.3 mas and 0.8 mas, respectively. The motion is predominately along the major axis of the source.

### 8.1. Slow motion of the jet with $v < 0.08c$

We searched for signs of a continuous slow motion in the source by fitting a straight line to the length of the major axis as a function of time. Neither in the case of the single component model nor in the case of the two-component model is the linear term significantly different from zero. The nominal values for the change of the major axis length with time are $-3 \pm 15$ $\mu$as yr$^{-1}$ in R.A. and $4 \pm 9$ $\mu$as yr$^{-1}$ in Dec., corresponding to $-50 \pm 250$ km s$^{-1}$ and $70 \pm 160$ km s$^{-1}$ respectively.

Is there coherent motion over shorter periods? Only during two periods early on, when our sampling was more frequent, did the variation in length appear smooth. The corresponding longitudinal speeds of the end of the jet (i.e. the point source) are close to zero during the first period from 1993 to 1994 and to 0.7 mas yr$^{-1}$ (12,000 km s$^{-1}$, 0.04$c$) during the second period from 1994 to 1995. This latter motion corresponds in Figure 7 to the long connecting line from a distance of 0.4 mas to 1.1 mas from the center. Three representative images of M81* during this period are displayed in Figure $2b-d$. The lengthening of the jet is obvious. For later epochs the time interval

between observations was longer and likely prevented us from temporally resolving the motion. The fastest length changes occurred between Dec. 1995 and Apr. 1996 and correspond to an outward motion of $0.075c$.

It is interesting that the transverse velocities for the end of the jet, implied by the changing p.a. and the (projected) length of the jet, are of the same order of magnitude as the longitudinal speeds during the period (i.e. 1993.5 to 1994.5) when the p.a. of the point source is changing. If we assume that the temporally unresolved motions of the end of the jet at later times are not significantly higher than the temporally resolved motions at earlier times, we find that the end of the jet moves in any direction on the sky with velocities of up to $0.08c$. These velocities are large in comparison to the velocity bound of the core, but small in comparison to relativistic velocities commonly observed for jet components.

### 8.2. Fast motion in the jet with $v > 0.25c$

It is remarkable that during large total flux density changes there is comparably little, if any, change in the structure. In particular for relatively large flux density increases over short time intervals, e.g. 50% between 15 March and 22 April 1994, the length and orientation of the single as well as the two-component Gaussian model do not change significantly. The increase in brightness must be spread out equally over most of the area represented by the dominant Gaussian. The speed must then be at least that given by the effective size of the Gaussian divided by the time interval between the epochs. Tests with a model show that the flux density needs to spread over $> 75\%$ of the FWHM of the Gaussian in order for the apparent change in the size of the Gaussian to be less than our standard errors of $\sim 10\%$. Therefore our lower limit for the speed with which the flux density is transported away from the core along the jet is 0.4 mas between the above two dates, which is equivalent to $0.25c$.

Given that the FWHM length varies quasi-randomly from epoch to epoch, with an rms of $\sim 20\%$, the lack of a significant change of the length could perhaps be a chance coincidence. The next largest flux density increases over short time intervals are 40% between 17 Dec. 1993 and 29 Jan. 1994 and 75% between 23 Dec. 1994 and 12 Feb. 1995, and again no significant change in the length of either of the two models was found. The fact that none of the sudden increases in flux density in our data are accompanied by a significant change in size suggests that our lower limit on the speed is realistic.

Even more rapid variations in flux density are reported by Ho et al. (1999). If they also occurred without any accompanying structural changes then an even faster transportation speed in the jet would have to be inferred. The fastest variation they report, $60 \pm 30\%$ per day, would be equivalent to a lower bound on the speed of $4c$. However, as mentioned in §4, our observations do not confirm such large intraday variations.

We also searched our VLBI data for direct signs of extremely rapid outward motion within an

individual observing run. We monitored the position of the point source on timescales of several hours by splitting datasets into several segments and using model fits for each segment, but no coherent outward motion was found, giving a $2\sigma$ upper bound for any such motion of $14c$.

## 9. Discussion

Twenty epochs of observations of the nucleus of M81 phase-referenced to a physically unrelated source in the same galaxy have significantly advanced our knowledge of this galaxy's center. At a distance of only 3.63 Mpc, M81 is the nearest spiral with an AGN and therefore of particular interest for the study of our own Galaxy's central source. In fact M81 is, besides Cen A, the nearest galaxy with an AGN altogether. But despite its closeness the nucleus can be only partly resolved even with the longest interferometer baselines on earth.

Previously we reported on the basic size, elongation, and orientation of the source structure and their dependence on frequency as well as on the evidence that the brightness decreases towards the NE (Paper I, B82). The source structure remained remarkably unchanged from one observation in 1981 to the start of our observations in 1993. We tentatively interpreted the results in terms of a core with a bent jet. The present observations draw a clearer picture of the nuclear source. Phase-referenced mapping enabled us to identify, with a standard error of only 600 AU, a stationary point. This point, located SW of the peak of the brightness distribution, is most likely the location of the core. The velocity within our galactic frame of reference is only $\leq 730$ km s$^{-1}$($2\sigma$ upper bound).

The uniqueness within the galaxy of M81* and the relatively low velocity limit of the stationary point in it suggests that it is associated with the putative black hole in the gravitational center of the galaxy. In our Galaxy, stars with velocities as high as $\sim 1,000$ km s$^{-1}$ have been found within 0.01 pc of Sgr A* (Genzel et al. 1997). Only Sgr A* itself appears to be at rest, having a proper motion with respect to extragalactic sources of $\lesssim 20$ km s$^{-1}$ (Reid et al. 1999), which is consistent with the expectation for a supermassive black hole in the center of our Galaxy. Similarly, M81* having a stationary point in its structure is consistent with the expectation for such a black hole in the center of M81.

This identification of the core is important for further studies of the core-jet system of M81*, for instance to determine unambiguously the spectrum of the core and the spectral index distribution of the jet (for a preliminary discussion see Ebbers et al. 1998).

The identification of the core is also important for studies of SN1993J. We have now found a stable reference point within M81* — the gravitational center of the galaxy — with which we can determine with the highest accuracy possible the position of the explosion center of SN1993J and investigate the expansion of the supernova with respect to it.

Furthermore, the identification of the core will become important for efforts to determine the

proper motion of the galaxy M81 in the extragalactic reference frame, which would have implications for models of the dynamics of nearby galaxies. No proper motion of any galaxy has yet been measured, but the stationary core in the gravitational center of M81 is the ideal source to measure such a proper motion given a sufficient time baseline of $\gtrsim 20$ years.

The remaining part of the structure varies in length and orientation about the core, and is therefore identified with the jet. The orientation of the jet displays the smoothest variations, with a timescale of $\sim$ 1 yr. Occasionally the jet bends by about 20° towards the east. This bending is consistent with the previously reported increase in size and p.a. of the source towards lower frequencies. The length of the jet varies less smoothly, with the end of the jet moving longitudinally with (projected) velocities of $< 0.08c$. The end of the jet also moves transversely, with similar velocities.

The most erratic variations occurred for the flux density of the dominant Gaussian (and the total flux density of M81*, which is dominated by the latter). Refractive interstellar scintillation can be excluded as the cause of the variations, since for a source size of say 0.3 mas it could account for variations of at most a few percent at 8.3 GHz (Rickett 1986). Our flux density variations are much larger and thus clearly intrinsic to the source. We can further conclude that the structural variations are also intrinsic to the source, since they are equivalent to local brightness changes of more than a few percent, and since they are non-random from epoch to epoch.

The hypothesis that the energy source for galactic nuclei is a starburst has been advanced by Terlevich et al. (1992). We showed in Paper I that such a hypothesis is untenable for the center of M81* because of its compactness and low average expansion velocity. Recently, Wrobel (1999) has shown that the starburst hypothesis is unlikely for another low level AGN, NGC5548, on the grounds of the astrometric stability of the radio nucleus. We note that in this paper we have shown that the motion of M81* is more than 20 times less than the upper limits for NGC5548 measured by Wrobel (1999), and this only strengthens our conclusion from Paper I that the starburst hypothesis is not applicable to M81*.

How do these results fit into the framework of the core-jet models of M81* suggested by previous observations? In early investigations M81* was modelled as an optically thick synchrotron self-absorbed source. It was interpreted as consisting of either one component elongated approximately along the rotation axis of the galaxy with magnetic field and electron energy density distribution declining along it, or as a few homogeneous condensations along the same axis, each becoming optically thick at a different frequency (B82, see also de Bruyn et al. 1976).

In Paper I we concluded that a bent, steep-spectrum jet probably oriented towards the NE was the most natural interpretation of the VLBI observations. We applied to M81* a model of Sgr A* developed by Falcke, Malkan & Biermann (1995) on the basis of Blandford & Königl's (1979) model of an optically thin unconfined jet. This allowed us to infer that the inclination angle of the jet is $\geq 30°$, and the accretion rate is $\sim 10^{-5.5}$ $M_\odot$ $yr^{-1}$.

Both Falcke (1996) and Böttcher, Reuter & Lesch (1997) have since modelled the VLBI data

for M81* in more detail. In their models, the source consists of a combination of jet condensations, which fade as they move outward and expand freely. The jet condensations are expected to move relativistically, consistent with our lower limit on the transport speed of $0.25c$. The overall source size is expected to increase with frequency $\propto \nu^{-0.8}$ as observed in Paper I. The lifetime of the condensations is short: applying the same parameters as Böttcher et al. (1997), we calculate from the present results that it is only about two weeks. As the time between our observations is longer than two weeks, we expect to see a completely different set of condensations at each epoch, and thus we would not expect to detect any direct outward motion of jet condensations. Instead we would expect rapid variation in the length of the jet, which we indeed observe. The total flux density, i.e. the sum of the flux densities of the individual condensations, would be expected to vary on a timescale of the lifetime of the condensations — again, about two weeks. This is also consistent with both our observations and those of others (Crane et al. 1976; Ho et al. 1999).

In contrast, the smoother variations observed for the orientation of the jet and occasionally for its length suggest changes which are distinct from the fast flow of jet condensations or the plasma. They could for instance be caused by precession of the central engine. It is also possible that they reflect the changing orientation and perhaps geometry of a variable channel or tube along which the ejected condensations are traveling. In other words, the plasma flows relativistically through a more slowly changing channel.

A possible geometric scenario is that the source behaves somewhat like a garden hose, fixed at one end, but free to move at the other. The fixed end of the hose represents the end of the jet near the core. The plasma flows through the hose with a high velocity, i.e. $> 0.25c$, and becomes fainter as it moves outward. The rate of injection at the core is rapidly variable, and this rapid variation will cause the observed total brightness and likely the illuminated length to vary erratically. In addition the orientation of the garden hose itself varies, possibly driven by the rapid variability of the flow. However this variation occurs more slowly, and this slower variation causes the observed smooth changes of the orientation of the jet. It also causes smooth changes of the length of the jet as a projection effect, since the variation of the orientation of the garden hose is unlikely to be confined to the plane of the sky, and so a change in the orientation would in general also cause the projected length of the garden hose to vary. Thus in addition to any rapid variations in length caused by the rapid flow variability, there would be smoother variations in projected length caused by the changing orientation of the hose. It is these last variations which would account for the observed episodes of smooth evolution in length.

With the core-jet scenario now firmly established for M81*, we can see general similarities to the more powerful core-jet systems in other AGN. The latter are mostly one-sided, as is M81*. In fact, only very few AGN have been shown to have counter-jets. A counter-jet in M81* cannot be excluded particularly because some emission has been detected with the VLA in the SW at a distance of $\sim 0.1$ pc from the core (Bartel et al. 1995). However, taking the uncertainty of the core position into account, any VLBI counter-jet in M81* would have a flux density of $\lesssim 20\%$ of that of the remaining source at 8.3 GHz. As in many AGN, most of the flux density of M81* comes from

the jet. We estimate that a compact core must have a flux density of $\lesssim 23\%$ of that of the source, so that the jet to counter-jet ratio is $\gtrsim 2.7$.

In terms of the length of the jet and the estimated accretion rate of a jet-disk model, M81* is a scaled-down version of the AGN of radio galaxies and quasars, which are several orders of magnitude more powerful. The length scale of M81* is two to three orders of magnitude shorter and the accretion rate is more than three orders of magnitude lower. The timescale of ejection for M81* must be relatively short, since we show that the energy transport times are less than a few weeks. Therefore, in order to keep the source illuminated, the ejection of new condensations has to happen with a timescale at least this short if not shorter. Such a period is at least an order of magnitude shorter than that observed for more powerful AGN. Therefore, observations of M81* may provide us with a glimpse of the effectively long-term evolution of an AGN, since we can observe M81* over a large number (i.e.$>$ 100) of condensation ejections. Knowledge of the long-term behavior, along with the scaling over several orders of magnitude in size and accretion rate could provide important additional constraints for models of AGN.

On the other hand, M81* appears in some respects to be a scaled-*up* version of the nucleus of our own Galaxy, Sgr A*. M81* has a radio power four orders of magnitude higher than Sgr A*. Its jet is much longer, having a length of 400 AU at 43 GHz (extrapolated from measurements of 700 AU at 22 GHz in Paper I). At this frequency, Lo et al. (1998) find an intrinsic major axis size of only $\sim 4$ AU for Sgr A* (see also Krichbaum et al. 1998). Therefore, the jet in M81* is at least two orders of magnitude larger than that of Sgr A*. The accretion rate in M81* is estimated to be about the same as that of Sgr A* (Narayan et al. 1998) or one to two orders of magnitude larger (see e.g. Falcke, Mannheim & Biermann 1993).

Thus it appears that in terms of power, jet length, and perhaps accretion rate, M81* is intermediate between the AGN of radio galaxies and quasars on the one hand and Sgr A* on the other hand, and therefore investigations of it may help shed some light on the largely hidden center of our own Galaxy as well.

## 10. Conclusions

Here we list a summary of our main conclusions:

1. A stationary point in the structure of the nucleus of M81 — identified with the core — was found south-west of the peak of the brightness distribution and located with a standard error of about 600 AU. Over 4 1/2 years, the $2\sigma$ upper bound on its average velocity in a non-rotating galactic reference frame is 730 km s$^{-1}$ (or 40$\mu$as yr$^{-1}$).

2. A short one-sided jet, variable in orientation and length, emanates from the core towards the north-east, in projection approximately along the rotation axis of the galaxy.

3. The orientation of the jet varies slowly on a timescale of about 1 year, with an rms of 6° about the mean of 50° for the inner part, and 12° about the mean of 60° for the outer part.

4. The length of the jet varies more quickly. While some consistent changes with timescales of $\sim 1$ year are observed, more rapid fluctuations are also observed. The mean length of the jet at 8.3 GHz is about 1.0 mas with an rms of 0.2 mas. Occasionally the jet appeared somewhat bent counterclockwise. The changes in both the length and the position angle of the jet imply that the end of the visible jet moves with projected velocities, both longitudinal and transverse, of $\lesssim 0.08c$. No significant outward motion was found over the 12 to 18h span of a typical observing run, giving a $2\sigma$ upper bound on rapid motions of $14c$.

5. The flux densities of the dominant component as well as the total flux density of the source varied erratically, with the time scale for total flux density variations being less than a few weeks.

6. Large flux density variations over only a few weeks did not affect the structure of the source, thus the increase in flux density must be spread equally throughout the source on a short timescale. The inferred lower bound on the plasma flow is $0.25c$.

7. In one particular case, we can infer a fast plasma flow of $> 0.25c$, and yet we measure smooth motions of $< 0.08c$ for the end of the visible jet. This is, to our knowledge, the only case, of observational evidence for a fast plasma flow and a slow pattern motion in the same jet at the same time.

8. The rapid variability of the length and the flux density of the jet are what is expected from relativistically moving, short-lived condensations, or condensations in an unsteady flow of plasma, ejected from the core on timescales less than a few weeks. The slow variability of the jet orientation points to a possible precession of the central engine or to slow changes in the orientation of a channel through which the condensations travel.

9. The core-jet in M81 may be a scaled-up version of the largely hidden nucleus in our own Galaxy and could provide a link between it and the more powerful AGN in radio galaxies and quasars.

10. From an astrometric point of view, the core in the nuclear radio source in M81 will become important as a reference point, with implications for studies of the radio spectrum of the jet, for the identification of the explosion center of SN1993J and the "absolute" measurement of its expansion velocity, and for the determination of the proper motion of the gravitational center of M81 in the extragalactic reference frame and thus the study of the dynamics of nearby galaxies.

ACKNOWLEDGMENTS. We thank V.I. Altunin, A.J. Beasley, W.H. Cannon, J.E. Conway, R. Freedman, D.A. Graham, D.L. Jones, A. Rius, G. Umana, and T. Venturi for help with several aspects of the project. Research at York University was partly supported by NSERC. The AIPS

model-fitting routine OMFIT was written by K. Desai. The NASA/JPL DSN is operated by JPL/Caltech, under contract with NASA. We have made use of NASA's Astrophysics Data System Abstract Service.

Table 1. 8.3 GHz VLBI Observations of M81*

| Date | Antennas[a] | Total time[b] | On-source baseline-hrs[c] | Recording mode[d] |
|---|---|---|---|---|
| 17 May 93 | Eb YBrFdHnKp MkNlOvPtSc | 9.6hrs | 10 | III-B |
| 19 Sep 93 | Mc RoAq YBrFdHnKpLaMkNlOvPtSc | 17.6hrs | 55 | III-B |
| 6 Nov 93 | EbMc Ro YBrFdHnKpLaMkNlOvPtSc | 18.0hrs | 26 | III-B |
| 17 Dec 93 | EbMc Go Aq YBrFdHnKpLaMkNlOvPtSc | 18.0hrs | 19 | III-B |
| 29 Jan 94 | Eb GoRoAq YBrFdHnKpLa NlOvPtSc | 17.6hrs | 23 | III-B |
| 15 Mar 94 | Eb Nt Ro GbYBrFdHnKpLaMkNlOvPtSc | 18.4hrs | 101 | III-B |
| 22 Apr 94 | Eb NtGoRo GbYBrFdHnKpLaMkNlOvPtSc | 16.9hrs | 59 | III-B |
| 21 Jun 94 | Eb NtGoRo GbYBrFdHnKpLaMkNlOvPtSc | 16.1hrs | 102 | III-B |
| 30 Aug 94 | Eb Nt Ro YBrFdHnKpLaMkNlOvPtSc | 14.8hrs | 49 | III-B |
| 31 Oct 94 | McNt RoAq YBrFdHnKpLaMkNlOvPtSc | 15.1hrs | 56 | III-B |
| 23 Dec 94 | Eb NtGoRoAqGbYBrFdHnKpLaMkNl PtSc | 16.1hrs | 106 | III-B |
| 12 Feb 95 | EbMcNtGoRoAqGbYBrFdHnKpLaMkNlOvPtSc | 11.8hrs | 190 | III-B |
| 11 May 95 | YBrFdHnKpLaMkNlOvPtSc | 15.4hrs | 24 | 128-4-2 |
| 17 Aug 95 | YBrFdHnKpLaMkNlOvPtSc | 14.2hrs | 50 | 128-4-2 |
| 19 Dec 95 | Ro YBrFdHnKpLaMkNlOvPtSc | 15.7hrs | 46 | 128-4-2 |
| 8 Apr 96 | GoRo Y FdHnKpLaMkNlOvPtSc | 7.4hrs | 79 | III-B |
| 1 Sep 96 | Eb YBrFdHnKpLaMkNlOvPtSc | 16.4hrs | 64 | 128-4-2 |
| 14 Dec 96 | Eb YBrFdHnKpLaMkNlOvPtSc | 17.2hrs | 97 | 256-8-2 |
| 7 Jun 97 | Eb GbYBrFdHnKpLaMkNlOvPtSc | 17.2hrs | 97 | 256-8-2 |
| 15 Nov 97 | EbMcNtGoRo GbYBrFdHnKpLaMkNlOvPtSc | 13.8hrs | 196 | 256-8-2 |

[a] Eb= 100m, MPIfR, Effelsberg, Germany; Mc= 32m, IdR-CNR, Medicina, Italy; Nt= 32m, IdR-CNR, Noto, Italy; Go= 70m, NASA-JPL, Goldstone, CA, USA; Ro= 70m, NASA-JPL, Robledo, Spain; Aq= 46m, CRESTech/York Univ. and Geomatics/NRCan, Algonquin Park, Ontario, Canada; Gb= 43m, NRAO, Green Bank, WV, USA; Y = equivalent diameter 130m, NRAO, near Socorro, NM, USA; Br= 25m, NRAO, Brewster, WA, USA; Fd= 25m, NRAO, Fort Davis, TX, USA; Hn= 25m, NRAO, Hancock, NH, USA; Kp= 25m, NRAO, Kitt Peak, AZ, USA; La= 25m, NRAO, Los Alamos, NM, USA; Mk= 25m, NRAO, Mauna Kea, HI, USA; Nl= 25m, NRAO, North Liberty, IA, USA; Ov= 25m, NRAO, Owens Valley, CA, USA; Pt= 25m, NRAO, Pie Town, NM, USA; Sc= 25m, NRAO, St. Croix, Virgin Islands, USA.

[b] Maximum span in hour angle at any one station.

[c] Sum over all the baselines of the number of hours spent on M81* after data calibration and editing.

[d] Recording mode: III-B= Mk III mode B double speed;
128-4-2= VLBA format, 128 MHz recorded in 4 base-band converters with 2-bit sampling.
256-8-2= VLBA format, 256 MHz recorded in 8 base-band converters with 2-bit sampling.

Table 2. Summary of the VLA Total Flux Density Measurements

| Date | Array Configuration | Flux Density[a] (mJy) |
|---|---|---|
| 17 May 1993 | B→C | 114 ± 6 |
| 19 Sep 1993 | DnC | 113 ± 6 |
| 6 Nov 1993 | D | 113 ± 6 |
| 17 Dec 1993 | D | 85 ± 4 |
| 29 Jan 1994 | D | 119 ± 6 |
| 15 Mar 1994 | A | 97 ± 5 |
| 22 Apr 1994 | A | 150 ± 8 |
| 22 Jun 1994 | B | 146 ± 7 |
| 30 Aug 1994 | B | 103 ± 5 |
| 31 Oct 1994 | C | 116 ± 6 |
| 23 Dec 1994 | C | 81 ± 4 |
| 12 Feb 1995 | C | 141 ± 7 |
| 11 May 1995 | D | 134 ± 8 |
| 17 Aug 1995 | A | 176 ± 9 |
| 19 Dec 1995 | B | 144 ± 7 |
| 8 Apr 1996 | C | 165 ± 9 |
| 1 Sep 1996 | D | 161 ± 8 |
| 14 Dec 1996 | A | 164 ± 8 |
| 7 Jun 1997 | AB | 119 ± 6 |
| 15 Nov 1997 | D | 189 ± 9 |
| Average, rms | | 132 ± 30 |

[a]The total flux densities of M81* with estimated standard errors including both statistical and systematic contributions.

Table 3. Summary of the VLBI model-fitting Results

| | | Single Component Model | | | Two Component Model | | | | | |
|---|---|---|---|---|---|---|---|---|---|---|
| | | Elliptical Gaussian | | | Elliptical Gaussian | | | Point Source | | |
| Date | $S$ | maj | min | p.a. | maj | min | p.a. | ratio | $r$ | $\theta$ |
| | (mJy) | (mas) | (mas) | (°) | (mas) | (mas) | (°) | (%) | (mas) | (°) |
| (1) | (2) | (3) | (4) | (5) | (6) | (7) | (8) | (9) | (10) | (11) |
| 17 May 93 | 114 | $0.44 \pm 0.03$ | $0.05^{+0.04}_{-0.12}$ | $59 \pm 3$ | $0.40 \pm 0.03$ | $0.18^{+0.03}_{-0.09}$ | $56 \pm 3$ | $5.3 \pm 1.0$ | $0.56 \pm 0.05$ | $74 \pm 3$ |
| 19 Sep 93 | 113 | 0.46 | 0.16 | 53 | 0.44 | 0.16 | 53 | 2.3 | 0.65 | 80 |
| 6 Nov 93 | 113 | 0.51 | 0.21 | 53 | 0.48 | 0.18 | 49 | 5.5 | 0.54 | 81 |
| 17 Dec 93 | 85 | 0.44 | 0.21 | 50 | 0.42 | 0.17 | 46 | 4.8 | 0.62 | 82 |
| 29 Jan 94 | 119 | 0.46 | 0.16 | 49 | 0.44 | 0.14 | 46 | 3.1 | 0.59 | 75 |
| 15 Mar 94 | 97 | 0.62 | 0.17 | 46 | 0.55 | 0.15 | 40 | 8.9 | 0.45 | 65 |
| 22 Apr 94 | 150 | 0.61 | 0.14 | 46 | 0.57 | 0.09 | 40 | 9.0 | 0.37 | 70 |
| 22 Jun 94 | 146 | 0.61 | 0.18 | 45 | 0.48 | 0.16 | 41 | 12.5 | 0.58 | 52 |
| 30 Aug 94 | 103 | 0.70 | 0.16 | 47 | 0.57 | 0.17 | 44 | 11.9 | 0.73 | 52 |
| 31 Oct 94 | 116 | 0.41 | 0.13 | 44 | 0.38 | 0.12 | 45 | 8.8 | 0.73 | 48 |
| 23 Dec 94 | 81 | 0.48 | 0.21 | 50 | 0.45 | 0.19 | 48 | 8.2 | 0.83 | 48 |
| 12 Feb 95 | 141 | 0.44 | 0.19 | 50 | 0.44 | 0.13 | 50 | 6.0 | 0.87 | 45 |
| 11 May 95 | 134 | 0.68 | 0.16 | 51 | 0.57 | 0.14 | 51 | 6.3 | 1.07 | 49 |
| 17 Aug 95 | 176 | 0.87 | 0.33 | 48 | 0.74 | 0.13 | 51 | 7.9 | 1.00 | 45 |
| 19 Dec 95 | 144 | 0.43 | 0.23 | 49 | 0.40 | 0.17 | 61 | 12.4 | 0.62 | 59 |
| 8 Apr 96 | 165 | 0.56 | 0.19 | 57 | 0.52 | 0.15 | 58 | 4.4 | 1.02 | 51 |
| 1 Sep 96 | 161 | 0.52 | 0.16 | 46 | 0.46 | 0.17 | 50 | 10.3 | 0.70 | 55 |
| 14 Dec 96 | 164 | 0.48 | 0.27 | 51 | 0.48 | 0.20 | 58 | 14.4 | 0.86 | 54 |
| 7 Jun 97 | 119 | 0.51 | 0.16 | 51 | 0.47 | 0.16 | 53 | 10.0 | 0.70 | 62 |
| 15 Nov 97 | 189 | 0.45 | 0.16 | 55 | 0.45 | 0.14 | 55 | 2.4 | 0.84 | 65 |
| average | 132 | 0.53 | 0.19 | 50 | 0.49 | 0.16 | 50 | 7.7 | 0.72 | 61 |
| rms | 30 | 0.11 | 0.05 | 4 | 0.08 | 0.03 | 6 | 3.4 | 0.18 | 12 |

The description of the columns is given below. The estimated standard errors include statistical and systematic contributions (see text, §6).

(1) The date (center time of the observing run).

(2) The total flux density of M81* at 8.3 GHz from simultaneous VLA observations (from Table 2, repeated here for convenience).

(3) The FWHM of the major axis of the elliptical Gaussian of the one component model.

(4) The FWHM of the minor axis of the elliptical Gaussian of the one component model.

(5) The p.a. of the major axis of the elliptical Gaussian of the one component model.

(6) The FWHM major axis of the elliptical Gaussian of the two component model.

(7) The FWHM minor axis of the elliptical Gaussian of the two component model.

(8) The p.a. of the major axis of the elliptical Gaussian of the two component model.

(9) The ratio of the flux density of the additional point source to the total flux density.

(10) The separation of the additional point source from the elliptical Gaussian.

(11) The p.a. of the position of the additional point source with respect to the elliptical Gaussian.

## REFERENCES

Baars, J. W. M., Genzel, R., Pauliny-Toth, I. I. K. & Witzel, A. 1977, A&A, 61, 99

Bartel, N., et al. 1982, ApJ, 262, 556, B82

Bartel, N., Herring, T.A., Ratner, M.I., Shapiro, I.I. & Corey, B.E. 1986, Nature, 319, 733

Bartel, N., et al. 1994, Nature, 386, 610

Bartel, N., et al. 1999, Science, *submitted*

Bartel N., Bietenholz, M. F. & Rupen, M. P. 1995, Nat. Acad. Sci., 92, 11374

Bietenholz, M. F., et al. 1996, ApJ, 457, 604 (Paper I)

Bietenholz, M. F., et al. 1994, in *Compact Extragalactic Radio Sources*, ed. J. A. Zensus & K. I. Kellermann, (Socorro: NRAO), 109

Bietenholz, M. F., Bartel, N., & Rupen, M. P. 1997, in *IAU Colloquium 164: Radio Emission from Galactic and Extragalactic Compact Sources*, ed. J. A. Zensus, J. M. Wrobel, and G. B. Taylor, 201

Blandford, R. D. & Königl, A. 1979, ApJ, 232, 34

Böttcher, M., Reuter, H.-P., & Lesch, H. 1997, A&A, 326, L33

Bower, G. A., Wilson, A. S., Heckman, T. M., & Richstone, D. O. 1996, AJ, 111, 1901

Crane, P. C., Giuffrida, T. S., & Carlson, J. B. 1976, ApJ, 203, L113

de Bruyn, A. G., Crane, P. C., Price, R. M. & Carlson, J. B. 1976, A&A, 46, 243

Ebbers, A., Bartel, N., Bietenholz, M. F. & Rupen, M. P. 1998, in *IAU Colloquium 164: Radio Emission from Galactic and Extragalactic Compact Sources*, ed. J. A. Zensus, J. M. Wrobel, and G. B. Taylor, 203

Elvis, M., & Van Speybroeck, L. 1982, ApJ, 257, L51

Falcke, H. 1996, ApJ, 464, L67

Falcke, H., Malkan, M. A., Biermann, P. L. 1995, A&A, 298, 375

Falcke, H., Mannheim, K., & Biermann, P. L. 1993, A&A, 278, L1

Freedman, W. L., et al. 1994, ApJ, 427, 628

Genzel, R., Eckart A., Ott, T. & Eisenhauer F. 1997, MNRAS, 291, 219

Ho, L. C., Filippenko, A. V. & Sargent, W. L. W. 1996, ApJ, 462, 183

Ho, L. C., Van Dyk, S. D., Pooley, G. G., Sramek, R. A. & Weiler, K. W. 1999, ApJ, 118, 843

Kaufman, M., Bash, F. N., Crane, P. C. & Jacoby, G. H. 1996, AJ, 112, 1021

Kellermann, K. I., Shaffer, D. B., Pauliny-Toth, I. I. K., Preuss, E., & Witzel, A. 1976, ApJ, 210, L121

Krichbaum, T. P. et al. 1998, A&A, 335, L106

Lo, K. Y., Shen, Z.-Q., Zhao, J.-H., & Ho, P. T. P. 1998, ApJ, 508, L61

Marcaide, J.M. & Shapiro, I.I. 1984, ApJ, 276, 56

Melia, F. 1992, ApJ, 398, L95

Narayan, R., Mahadevan, R., Grindlay, J. E., Pobhan, R. G., & Gammie, C. 1998, ApJ, 492, 554.

Peimbert, N. & Torres-Peimbert, S. 1981, ApJ, 245, 845

Reid, M. J., Readhead, A. C. S., Vermeulen, R. C. & Treuhaft R. N. 1999, *preprint*: astro-ph/9905075

Reuter, H.-P. & Lesch, H. 1996, A&A, 310, L5

Rickett, B. J. 1986, ApJ, 307, 564

Rioja, M.J., Marcaide, J.M., Elósegui, P. & Shapiro, I.I. 1997, A&A, 325, 383

Rots, A. H. & Shane, W. W. 1975, A&A, 45, 25

Terlevich, R., Tenorio-Tagle, G., Franco, J. & Melnick J. 1992 MNRAS, 255, 713

Wrobel, J. M. 1999, *preprint*: astro-ph/9910427

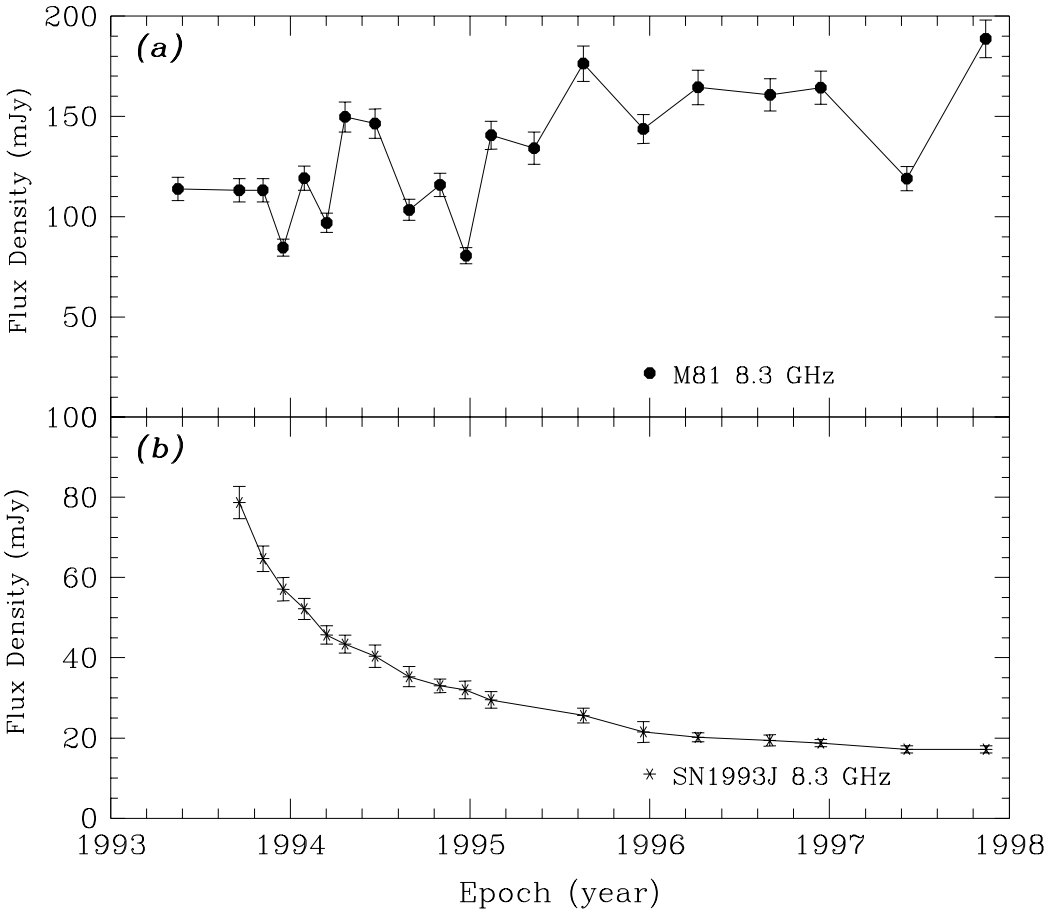


Fig. 1.— Total flux densities at 8.3 GHz derived from VLA imaging observations. In ($a$) we show the total flux density evolution of M81*. For comparison, in ($b$) we show the total flux density evolution of SN1993J which was obtained from the same imaging runs and which shows only the expected smooth decline, and does not exhibit the variability shown by M81*.

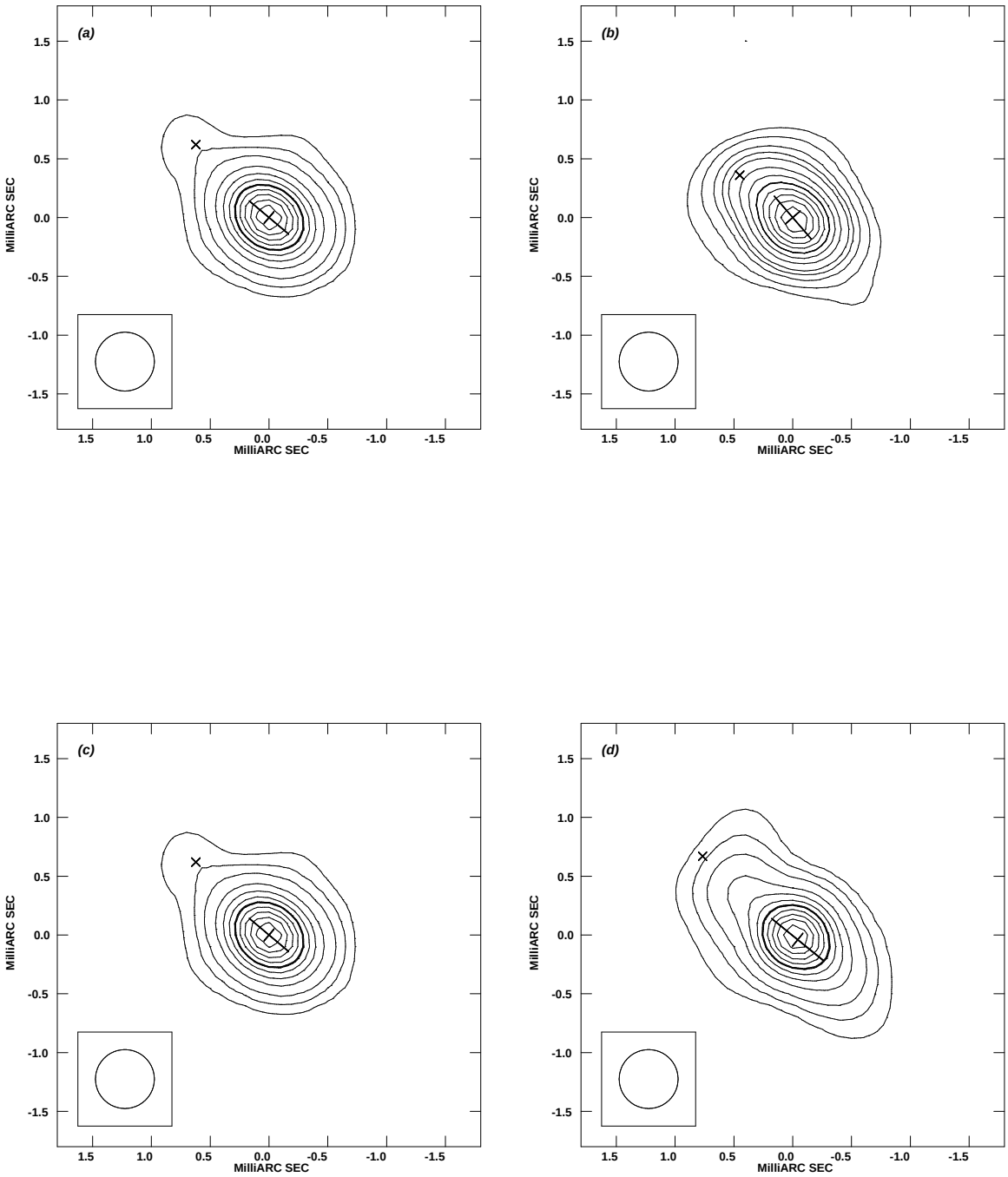
(a)
(b)
(c)
(d)
MilliARC SEC
1.5
1.0
0.5
0.0
-0.5
-1.0
-1.5

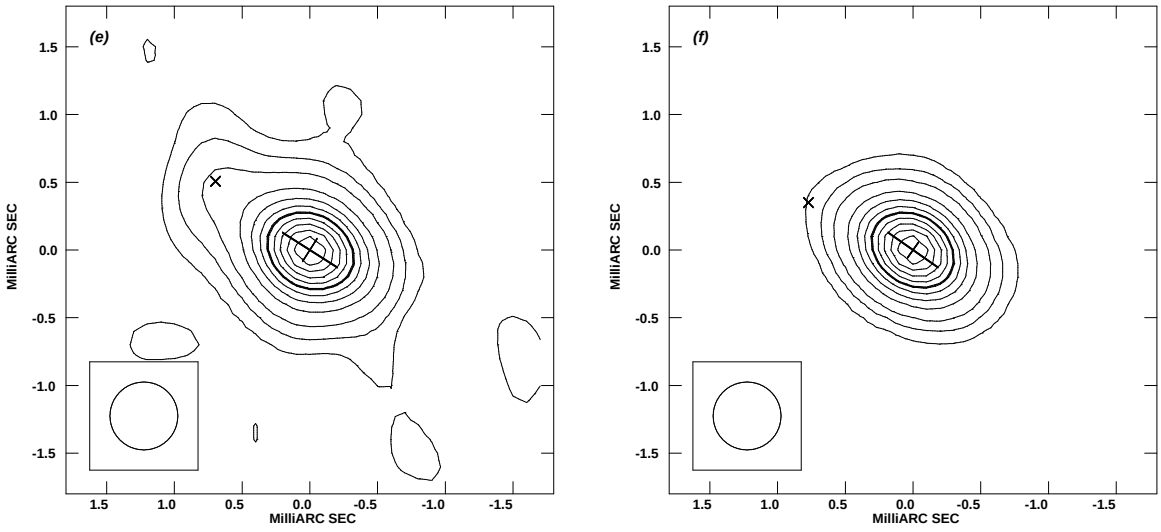


Fig. 2.— CLEAN images of M81* at 8.3 GHz. The contours are at 2, 5, 10, 20, 30, 40, **50**, 60, 70, 80 and 90% of the peak flux density (the 50% contour is indicated by a heavier line). North is up and east is to the left. Uniform weighting was used, and the images were convolved with a clean beam of FWHM 0.5 mas. For three images (see below) this beam represents a super-resolution by a factor $\leq 1.8$. However, because of the compactness of the source and the relatively high dynamic range of $> 200$ our maps should be reliable within the framework or our interpretations. Also indicated are the results of the two component model fit: the large cross shows the position, orientation and FWHM size of the fit elliptical Gaussian, and the small cross shows the position of the additional point source that was fit to the data. For each image, the observing date, the peak brightness, the background rms, and the flux density of the additional point source are given below. Lastly, in parentheses, we give the uniform-weighted beam parameters (FWHM major and minor axes, position angle) where its mean FWHM size was larger than 0.5 mas.
(*a*) May 17, 1993; 78 mJy/beam; ±0.27 mJy/beam; 6 mJy.
(*b*) June 21, 1994; 75 mJy/beam; ±0.29 mJy/beam; 18 mJy.
(*c*) Feb. 12, 1995; 101 mJy/beam; ±0.21 mJy/beam; 8 mJy ($0.90 \times 0.80$ mas at $-50°$).
(*d*) May 11, 1995; 99 mJy/beam; ±0.41 mJy/beam; 8 mJy ($0.90 \times 0.60$ mas at $55°$).
(*e*) Dec. 14, 1996; 90 mJy/beam; ±0.28 mJy/beam; 24 mJy ($0.80 \times 0.51$ mas at $-11°$).
(*f*) Nov. 15 1997; 118 mJy/beam; ±0.13 mJy/beam; 5 mJy.

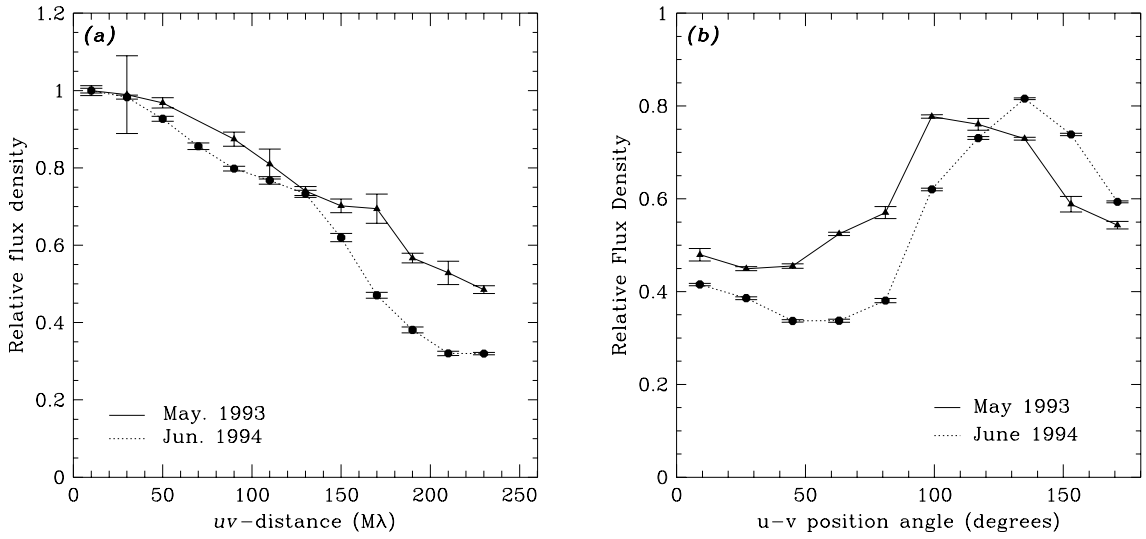


Fig. 3.— Part (*a*) shows the average visibility as a function of *u*-*v* distance. The solid line denotes the May 1993 data and the dashed line the June 1994 data, showing that the source is more extended in June 1994. Part (*b*) shows, for the same two epochs, the average visibility of M81* in an annulus with *u*-*v* distances between 200 M$\lambda$ and 260 M$\lambda$, as a function of *u*-*v* position angle. The maximum and minimum of the two curves are clearly displaced, indicating a shift in the p.a. of the major axis of the source.

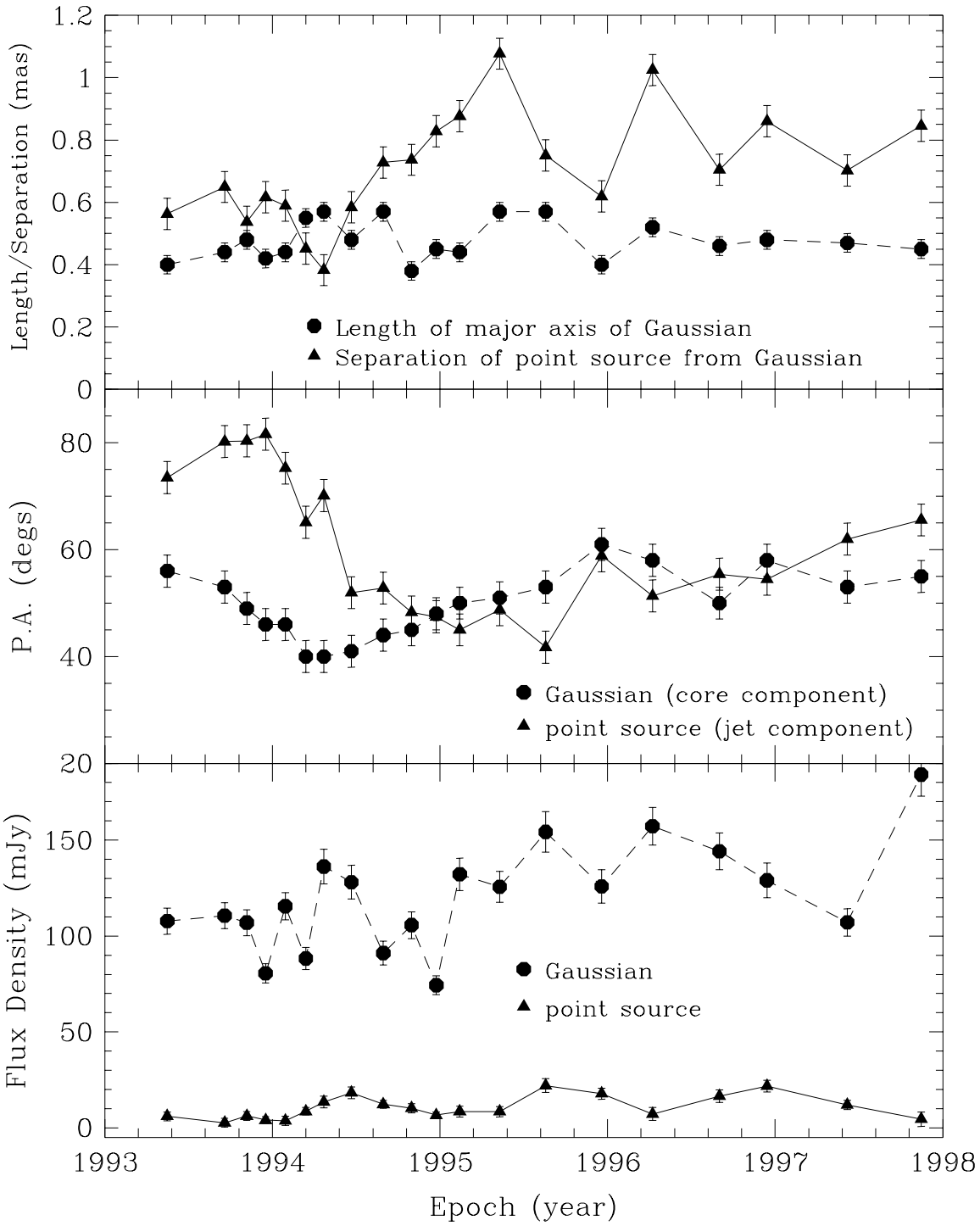


Fig. 4.— The variability of the parameters of M81* as a function of time. The parameters of the elliptical Gaussian are shown by circles, while those of the additional point source are shown by triangles. The top panel shows the FWHM of the major axis of the Gaussian and the separation of the point source from the Gaussian. The central panel shows the p.a. of the major axis of the Gaussian and the p.a. of the position of the point source with respect to the Gaussian. The lower panel shows the flux densities of the Gaussian and the point source (normalized to the total flux density measured at the VLA). The uncertainties shown are typical standard errors which include both statistical and systematic contributions (see text, §6).

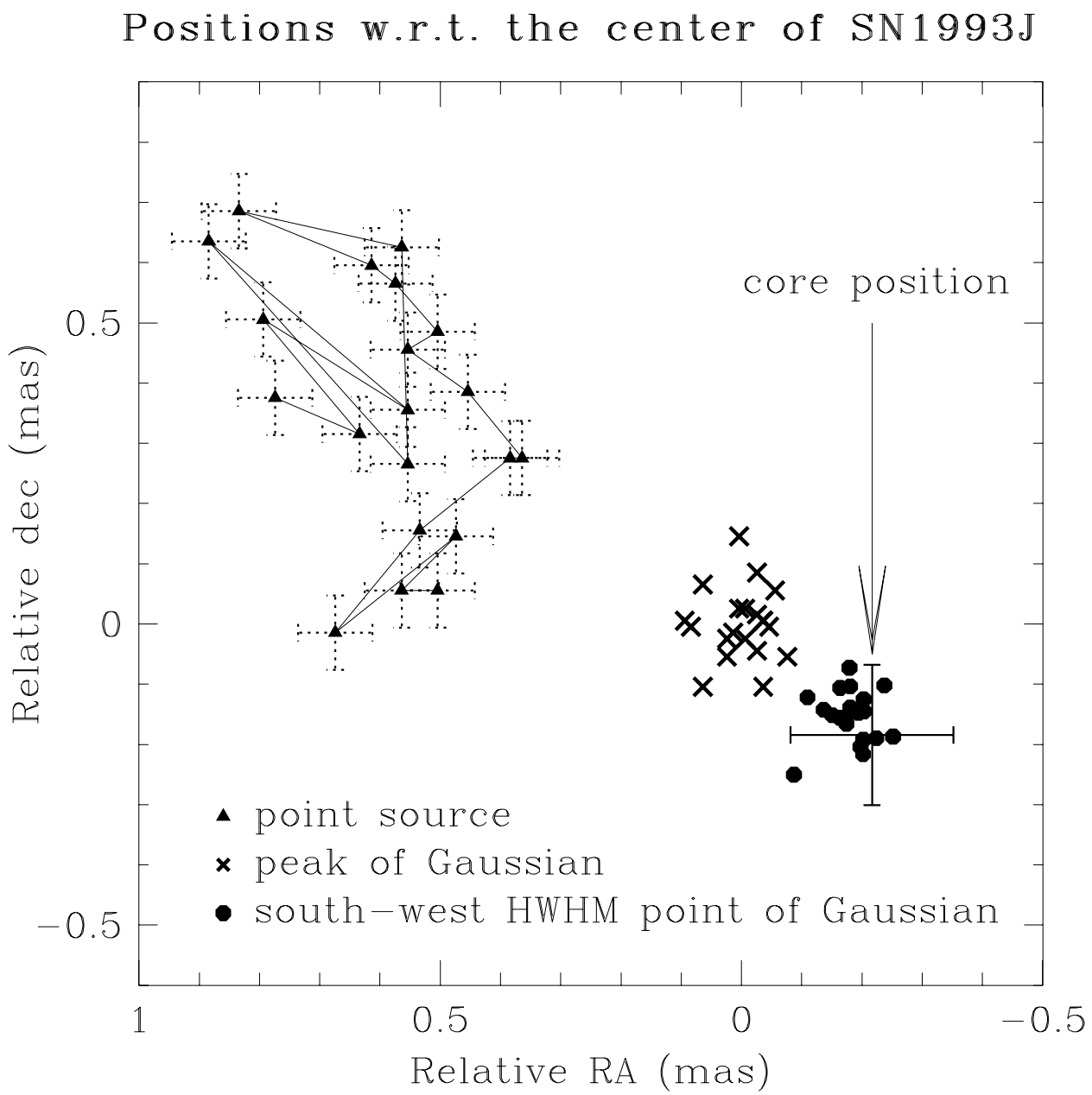


Fig. 5.— Positions at each epoch of three points in the two component model, plotted with respect to the geometric center of SN1993J. The three points are: *i*) the point source, shown by triangles, with the motion indicated by the connecting line where the lower right end of the line is the position in May, 1993; *ii*) the center position of the Gaussian, shown by the small crosses (with the standard errors of 50 $\mu$as omitted for clarity); and *iii*) the positions of the south-west HWHM point of the Gaussian, shown by the circles (again with the standard errors of 60 $\mu$as omitted for clarity). The origin is the mean position of the center of the Gaussian with respect to SN1993J. Also shown is the derived core position with its standard error.

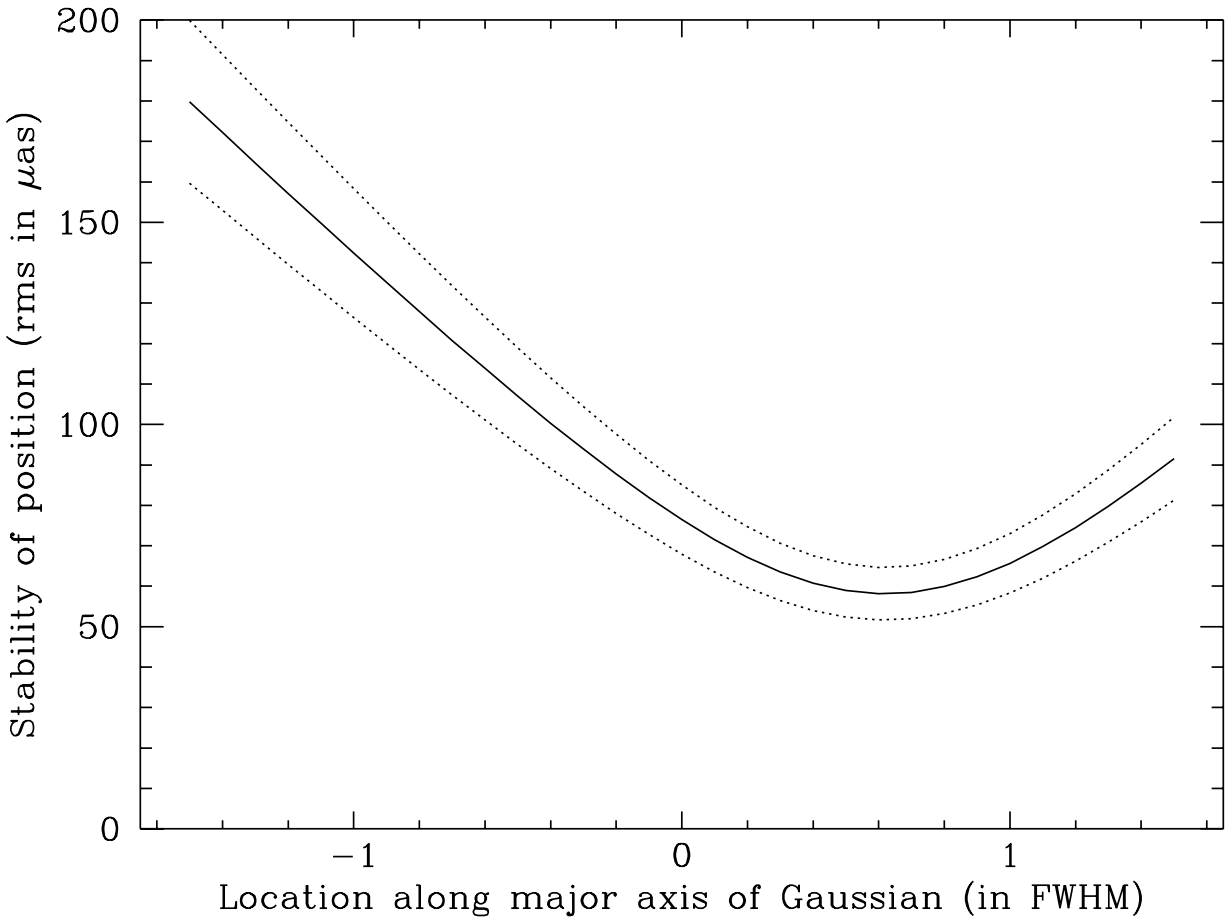


Fig. 6.— The solid line shows the variability in position of different locations along the major axis of the fit Gaussian. The variability is the rms in $\mu$as of the position on the sky of that particular location on the major axis of the Gaussian. The minimum variability indicates the position of the core along the major axis of the Gaussian. The standard errors of the rms variability are indicated by the dotted lines, from which the uncertainty of the core position is derived. The curve is smooth and continuous because the position, and thus the positional rms over 20 epochs, is functionally defined for any point along the major axis of the Gaussian.

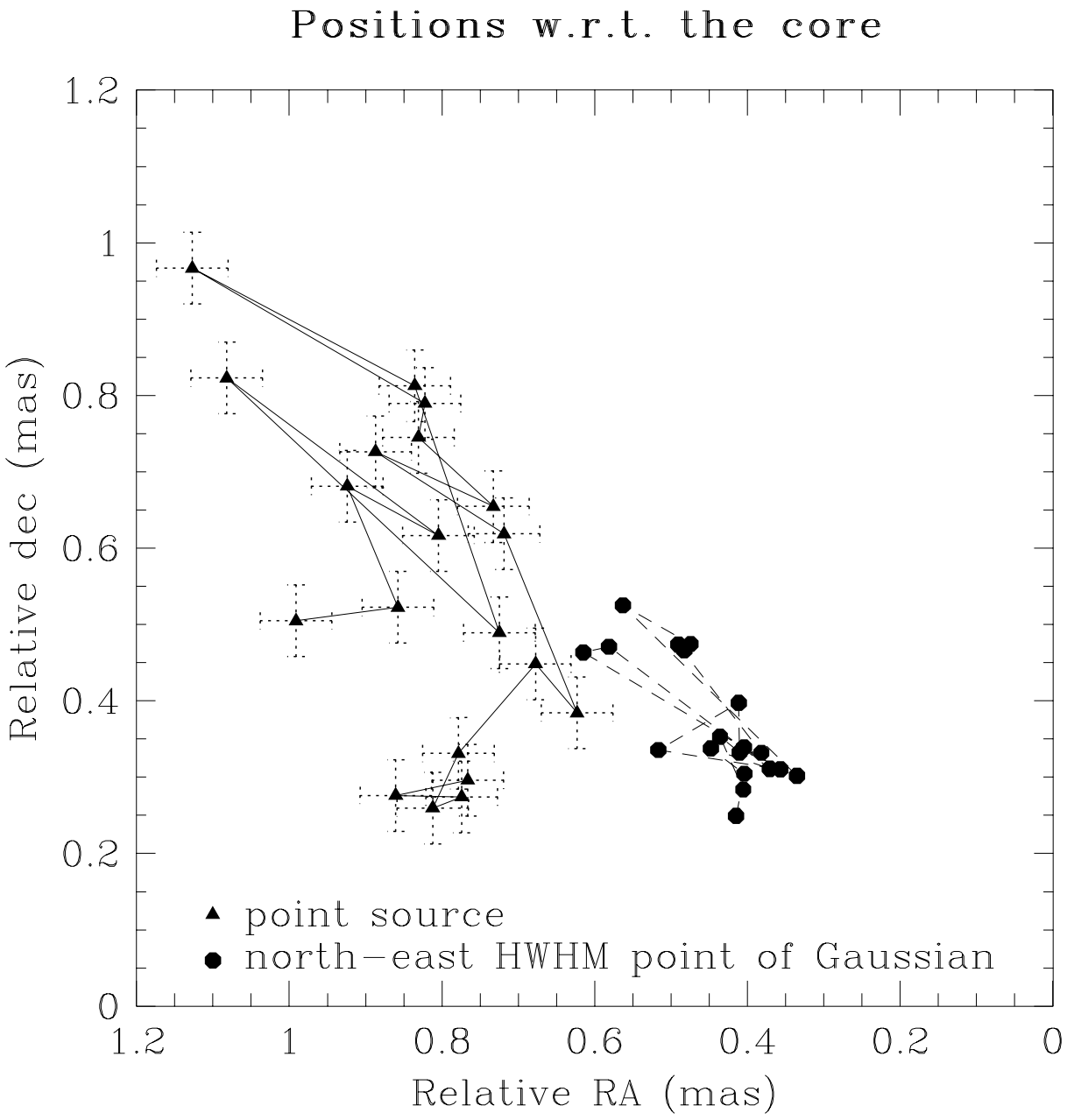


Fig. 7.— Positions at each epoch of two points in the two component model, plotted with respect to the core position. The triangles (connected by a solid line) show the positions of the additional point source, with the lower right end of the line indicating the position in May 1993, and the upper left end corresponding to the position in Nov. 1997. The circles, connected by a dashed line, show the positions of the north-east HWHM point of the Gaussian, i.e. that away from the core, over the same time period (with the standard errors of 30 $\mu$as omitted for clarity).